Angle-gathers by Fourier Transform

Paul Sava and Sergey Fomel[1]

ABSTRACT

In this paper, we present a method for computing angle-domain common-image gathers from wave-equation depth-migrated seismic images. We show that the method amounts to a radial-trace transform in the Fourier domain and that it is equivalent to a slant stack in the space domain. We obtain the angle-gathers using a stretch technique that enables us to impose smoothness through regularization. Several examples show that our method is accurate, fast, robust, easy to implement and that it can be used for real 3-D prestack data in applications related to velocity analysis and amplitude-versus angle (AVA) analysis.

INTRODUCTION

Traditionally, migration velocity analysis and AVO employ offset-domain common-image gathers, since most of the relevant information is not described by the zero-offset images. However, it is difficult to produce these gathers with wave-equation migration because the offset dimension of the downward continued data shrinks with depth. A solution to this problem is to use angle-gathers instead of offset-gathers. Angle-gathers also provide more straightforward information for amplitude analysis, that is, amplitude variation with angle (AVA) instead of the more common amplitude variation with offset (AVO).

Angle-domain common-image gathers are representations of the seismic images sorted by the aperture angle at the reflection point (Prucha et al., 1999a; Fomel and Prucha, 1999). In the space-domain, the reflection angles can be evaluated by the simple differential equation:

$$\tan\gamma = -\frac{\partial z}{\partial h}$$

where γ represents half of the aperture angle at the reflector, and z and $\vec{h}$ are, respectively, the depth and half-offset for the particular reflection (Figure 1).

Prucha et al. (1999a) evaluate wave-equation angle-domain common-image gathers (AD-CIG) by slant-stacking between the downward continuation and the imaging steps. They also produce their output as a function of offset ray-parameter (p) instead of the reflection angle (γ). However, angle-domain gathers do not need to be computed by slant stacks directly, but could be more easily evaluated in the Fourier-domain, with output in the true reflection angle,

[1]**email:** paul@sep.stanford.edu, sergey@sep.stanford.edu

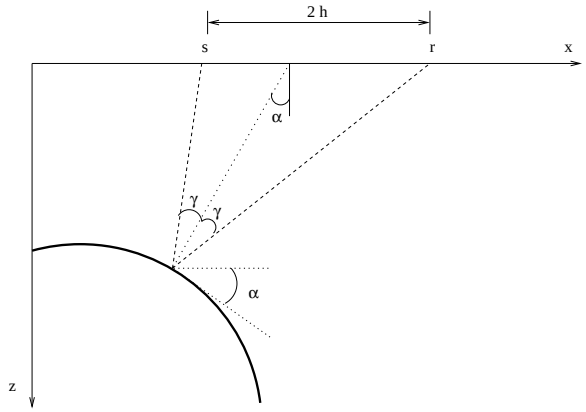

Figure 1: The geometrical relationship relating the reflection angle γ at the reflector, to the half-offset $\vec{h}$. agfft-rays [NR]

using the simple equation:

$$\tan\gamma = -\frac{|\vec{k}_h|}{k_z}. \tag{1}$$

which, in essence, is simply a stretch of the offset axis transformed in the Fourier-domain.

It is interesting to emphasize that this Fourier-domain method of computation of angle-gathers is a radial-trace transform. Ottolini (1982) shows that slant stacks are, in fact, generally equivalent to radial-trace transforms, with significant advantages and disadvantages for each of these two alternatives.

In this paper, we review the radial stretch theory and show that computing the ADCIGs using equation (1) is indeed equivalent to slant stacks but that it gives us the freedom to postpone the conversion to angle until after prestack wave-equation migration. This Fourier domain method makes it possible to convert seismic images easily from the offset-domain to the angle-domain without re-migrating the data.

The novelty of our method is that, in the Fourier-domain, the radial-trace transformation can be easily regularized, thus leading to smooth and continuous representations of the reflectors along the angle axis. A similar method of regularized stretch has been used in other applications: velocity continuation (Fomel, 1998), Stolt migration (Vaillant and Fomel, 1999), and Stolt residual migration (Sava, 1999b,a). It could also find many other applications, for example in coherent-noise removal using radial-trace transforms (Brown and Claerbout, 2000).

Our method of angle-gather computation is different from the slant-stack approach not only in the domain in which it operates, but also in the low cost involved, the robustness, and simplicity of the implementation. If we compute angle-gathers in conjunction with Stolt residual migration, this method becomes even more attractive since the seismic images are already transformed to the Fourier-domain, which makes the true cost of the transformation insignificant.

EQUIVALENCE TO SLANT STACKS

The Fourier-domain stretch represented by equation (1) is equivalent to a slant stack in the $z-\vec{h}$ domain. Indeed, we can convert an image gather in the offset-domain (**H**) to one in the angle-domain (**A**), using a slant-stack equation of the form

$$\mathbf{A}(z,\vec{\mu}) = \int \mathbf{H}\left(z+\vec{\mu}\cdot\vec{h},\vec{h}\right) d\vec{h}, \tag{2}$$

where $\vec{\mu}$ is a vector describing the direction of the stack.

Fourier transforming equation (2) over the depth axis, we obtain

$$\underline{\mathbf{A}}(k_z,\vec{\mu}) = \int \left[\int \mathbf{H}\left(z+\vec{\mu}\cdot\vec{h},\vec{h}\right) d\vec{h}\right] e^{ik_z z} dz$$

where the underline stands for a 1-D Fourier transform. We can continue by writing the equation

$$\underline{\mathbf{A}}(k_z,\vec{\mu}) = \int\int \mathbf{H}\left(z+\vec{\mu}\cdot\vec{h},\vec{h}\right) e^{ik_z\left(z+\vec{\mu}\cdot\vec{h}\right)-ik_z\vec{\mu}\cdot\vec{h}} d\vec{h}dz,$$

where we can re-arrange the terms as

$$\underline{\mathbf{A}}(k_z,\vec{\mu}) = \int \left[\int \mathbf{H}\left(z+\vec{\mu}\cdot\vec{h},\vec{h}\right) e^{ik_z\left(z+\vec{\mu}\cdot\vec{h}\right)} dz\right] e^{-ik_z\vec{\mu}\cdot\vec{h}} d\vec{h},$$

which highlights the relation between the 1-D Fourier-transformed angle-domain and offset-domain representation of the seismic images:

$$\underline{\mathbf{A}}(k_z,\vec{\mu}) = \int \underline{\mathbf{H}}\left(k_z,\vec{h}\right) e^{-ik_z\vec{\mu}\cdot\vec{h}} d\vec{h}.$$

We recognize on the right-hand side of the previous equation additional Fourier transforms over the offset axes, and therefore we can write

$$\underline{\mathbf{A}}(k_z,\vec{\mu}) = \underline{\underline{\underline{\mathbf{H}}}}(k_z,-\vec{\mu}k_z),$$

where the triple underline stands for the 3-D Fourier transform of the offset-domain common-image gather. Finally, defining $-\vec{\mu}k_z = \vec{k_h}$, we can conclude that the 1-D Fourier transforms of angle-domain gathers are equivalent to the 3-D Fourier transforms of the offset-domain gathers,

$$\underline{\mathbf{A}}(k_z,\vec{\mu}) = \underline{\underline{\underline{\mathbf{H}}}}\left(k_z,\vec{k_h}\right), \tag{3}$$

subject to the stretch of the offset axis according to the simple law

$$\vec{\mu} = -\frac{\vec{k_h}}{k_z}. \tag{4}$$

We can recognize in equation (4) the fundamental relation between the reflection angle and the Fourier-domain quantities that are evaluated in wave-equation migration. This equation also shows that the angles evaluated by (1) are indeed equivalent to slant stacks on offset-domain common-image gathers. Therefore, we could either compute angles for each of the two offset axes with the equations

$$\gamma_x = -\tan^{-1}\left(\frac{k_{hx}}{k_z}\right)$$
$$\gamma_y = -\tan^{-1}\left(\frac{k_{hy}}{k_z}\right),$$

or compute one angle corresponding to the entire offset vector:

$$\gamma = -\tan^{-1}\left(\frac{|\vec{k_h}|}{k_z}\right).$$

REGULARIZATION OF THE ANGLE DOMAIN

In essence, the angle-gather method, introduced in this paper, amounts to a stretch of the offset angle according to equation (4). The stretch takes every point on the offset wavenumber axis and repositions it on the angle axis, most likely not on its regular grid. We therefore need to interpolate the unevenly sampled axis to the regular one. In other words, we need to solve a simple linear interpolation problem

$$\mathbf{Lm} \approx \mathbf{d}$$

where the model (**m**) is represented by the evenly-spaced values on the angle axis, the data (**d**) is represented by the unevenly-spaced values on the angle axis, and (**L**) represents a 1-D linear interpolation operator. Since parts of the model space will not be covered because of the uneven distribution of the data, we need to regularize the interpolation process and solve a system such as

$$\mathbf{Lm} \approx \mathbf{d} \tag{5}$$
$$\epsilon\mathbf{Am} \approx 0 \tag{6}$$

where (**A**) represents a 1-D roughener operator. Consequently, the least-squares solution to the system (5) is

$$\mathbf{m} = \left(\mathbf{L}^T\mathbf{L} + \epsilon^2\mathbf{A}^T\mathbf{A}\right)^{-1}\mathbf{L}^T\mathbf{d}. \tag{7}$$

In the special case of the angle-domain stretch, the inverted term on the right side of equation (7) is a tridiagonal matrix. Given the sparseness of the stretched data, the least-squares tridiagonal matrix corresponding to the operator **L** has zeros present along the diagonals, which results in instability during inversion. However, the regularization term fills the gaps; therefore, the inversion of the matrix in equation (7) is well-behaved.

Since the matrix $\mathbf{L}^T\mathbf{L} + \epsilon^2\mathbf{A}^T\mathbf{A}$ is tridiagonal, we can invert it using a fast tridiagonal solver (Golub and Van Loan, 1989); Consequently, we obtain smoothly interpolated values for the ADCIGs. A similar approach could also be used for other problems, for example in Stolt migration (Vaillant and Fomel, 1999), residual migration (Sava, 1999b,a), or in velocity continuation (Fomel, 1998).

The main benefit of solving the least-squares problem this way is that we can obtain a very inexpensive regularized solution, with important benefits not only in data visualization, but also in other problems such as wave-equation migration velocity analysis (Biondi and Sava, 1999; Sava and Biondi, 2000) and imaging (Prucha et al., 1999b).

EXAMPLES

We exemplify the proposed method on two synthetic models and two real datasets.

The first example is a 2-D synthetic model with dipping reflectors at various angles. We generated the synthetic data using wave-equation modeling (Biondi, 1999). Next, we imaged the data, first using the correct and then using an incorrect velocity model, a slower velocity in this example. In the case of correct velocity, the ADCIGs are flat, but they are not flat in the case of the incorrect velocity model (Figure 2). Because the simulated acquisition is represented by wide offsets and the model is reasonably shallow, there is no significant decrease in the angular coverage at the deeper reflectors. However, the steep reflectors are characterized by smaller angular coverage due to the limited acquisition geometry.

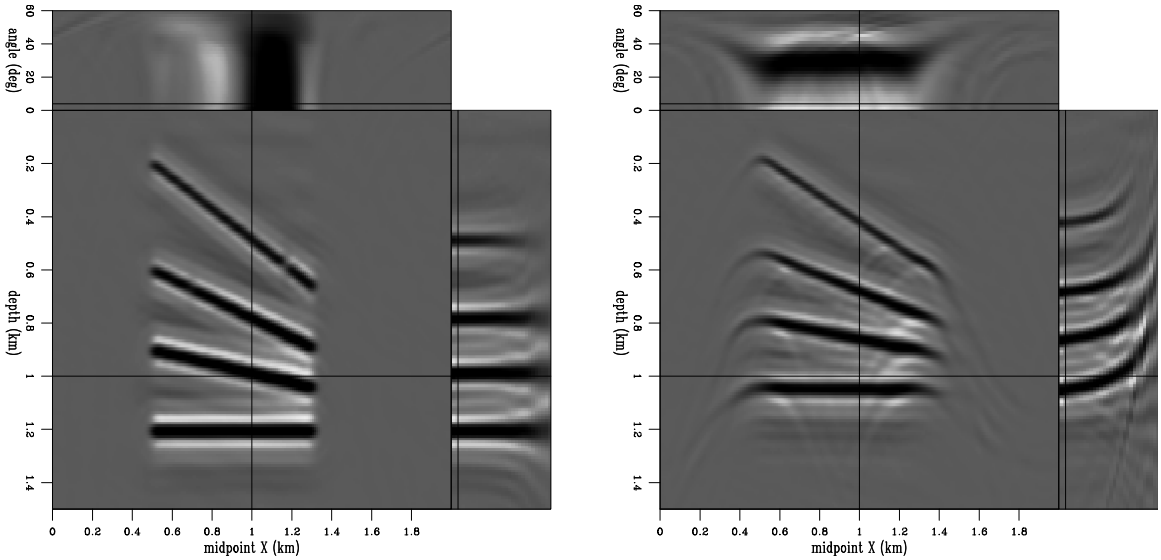

Figure 2: The first synthetic model. The reflectivity is composed of interfaces dipping at different angles. All the events are flat along the reflection angle axis, in the case where we use the correct velocity (left). However, when we use a wrong velocity model, the image loses focus and the ADCIGs bend (right). agfft-dipsynt.cig01 [NR]

In the second example, we consider a more complex synthetic model, centered on a salt body. The model was generated at Elf-IFP-CGG and inspired by real data recorded in the North Sea (Prucha et al., 1998). Again, we image both with a correct velocity model and an incorrect one (Figure3). The conclusions are similar to those in the first example: correct velocity flattens the events in the angle-domain common-image gathers, while incorrect velocity does not. Again, there is no significant decrease in the angular coverage at the deeper reflector.

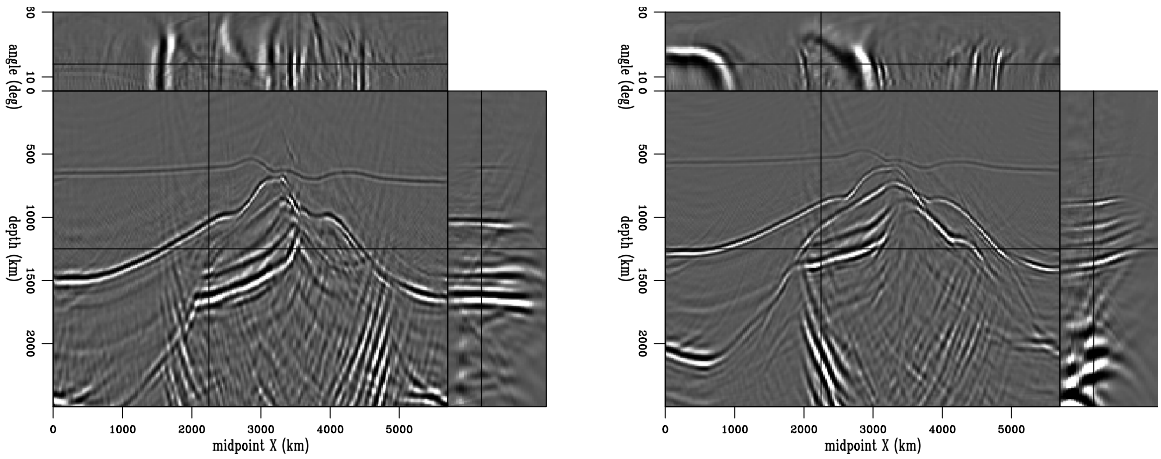

Figure 3: The second synthetic model, depicting a salt body. The ADCIGs show flat events when the velocity model is correct (left), but bend when the velocity is incorrect. agfft-saltsynt.cig01 [NR]

The third example is a real dataset acquired in a salt-dome region of the North Sea (Prucha et al., 1998; Vaillant and Sava, 1999). Figure 4 depicts a slice of the image taken at a small reflection angle, and the small panels at the top and the right represent ADCIGs. The image generated for this dataset goes much deeper compared to the preceding synthetics, and we see that the angular coverage decreases as the depth increases. Some of the events appear flat, while others are bending, indicating velocity inaccuracies.

It is apparent from the image that some of the events lose their sharpness and the relative contrast decreases. This is understandable, since the energy of every event is spread along the angle axis. The true migrated image could be recovered by summation along the angle axis (Figure 5).

This example enables us to analyze the efficiency of our regularization method. Figure 6 shows angle-domain common-image gathers for a particular midpoint. The left panel represents the result obtained without regularization ($\epsilon = 0.0$). In contrast, the panel on the right shows the result we obtain with regularization ($\epsilon = 1.0$). The regularized image is much cleaner, without visible distortions of the shape and amplitudes of the events. Since the noise level is much lower, we can easily identify faint events that would otherwise be impossible to discern, for example at depths greater than 4000 m.

Finally, a fourth example addresses the amplitude variation with angle analysis (AVA) issue. Our method produces the output as a function of the reflection angle, which makes it an

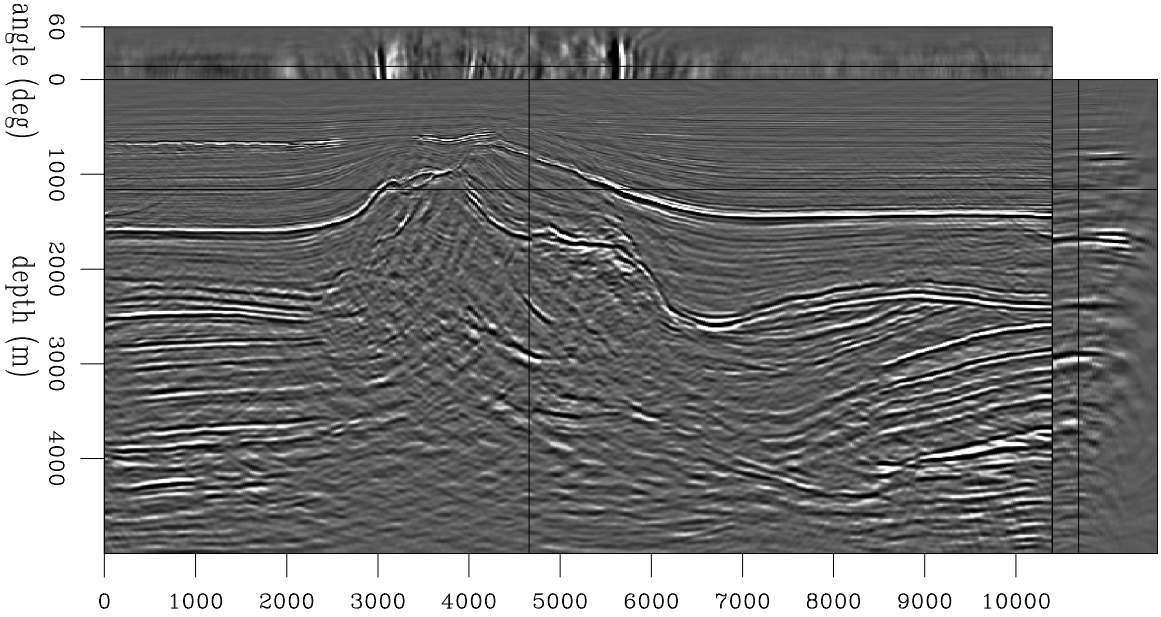

Figure 4: Migrated image for the North Sea dataset presented as ADCIGs. The ADCIGs are mostly flat, but they reveal the areas where the velocity map needs improvement. The image as a whole loses part of its sharpness, because the energy of each event is spread along the angle axis. agfft-saltreal.cig [NR]

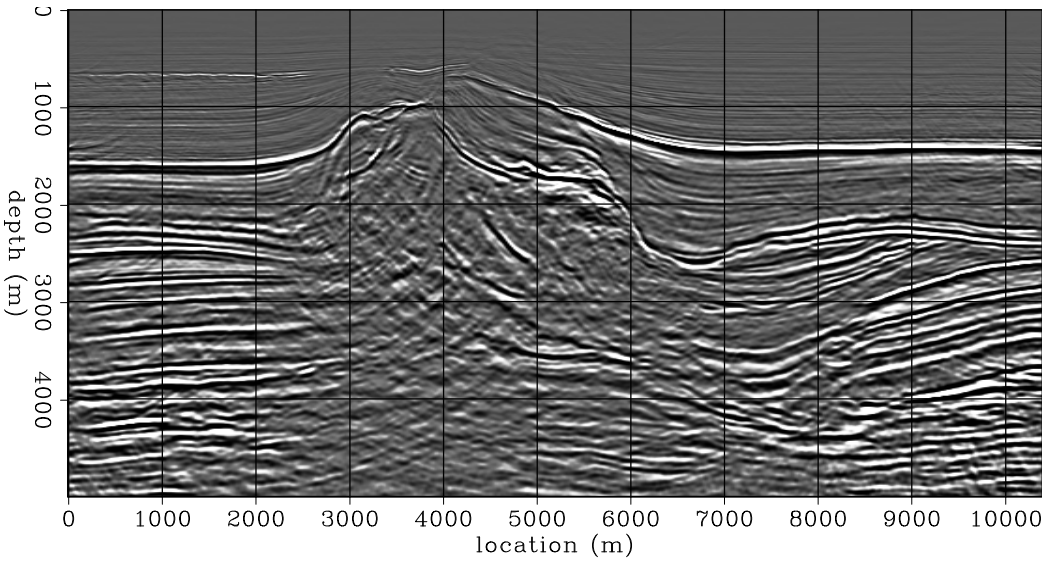

Figure 5: Migrated image for the North Sea dataset, stacked over the angle axis in the ADCIGs. agfft-saltreal.stk [NR]

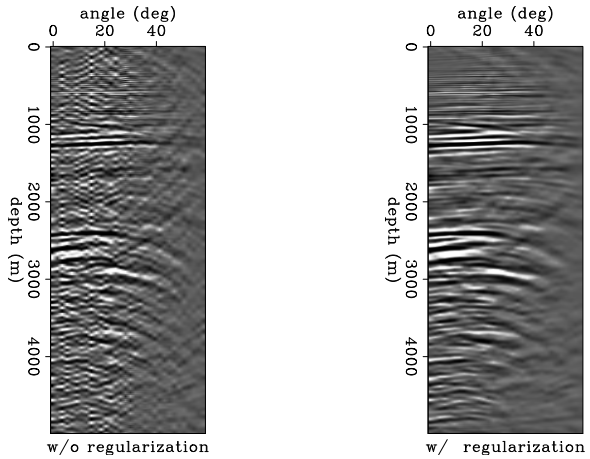

Figure 6: A comparison of ADCIGs with regularization (right panel) and without regularization (left panel). agfft-saltreal.eps [NR]

ideal tool for AVA analysis. The crucial question is how much the amplitudes are affected by the method, especially given that we impose a certain amount of smoothness through regularization. Previous research (Prucha et al., 1999a) indicates that ADCIGs obtained by wave-equation imaging have the potential to preserve AVA effects.

For the AVA example, we use a dataset from a gas-hydrates study, for which the AVO effects are significant (Ecker, 1998). Figure 7 represents the wave-equation migrated image, displayed as ADCIGs. Figure 8 shows 4 wiggle-plots of ADCIGs located around 45 km from the left origin of the survey. This area is particularly interesting since it captures both the bottom-simulation reflector (BSR) and the flat reflector from the hydrate-gas transition. The results confirm the amplitude trend variation previously highlighted for this dataset; specifically, we can observe significant amplitude increase as a function of angle, especially for the BSR. This result was obtained for a moderate choice of the regularization parameter ($\epsilon = 1.0$). Caution should be exercised in this matter, since a higher value could attenuate the amplitude of the variations. A more thorough and quantitative analysis awaits future research.

It is worth mentioning that, in certain applications, the amplitude variations with angle are undesirable. A good example is velocity-analysis where AVA effects can be misleading and indicate incorrect updates of the velocity model. However, we can perhaps control this by boosting the ϵ parameter, with the effect of attenuating the variations along angles.

DISCUSSION

Several key points highlight the strengths of our method of computing angle-domain common-image gathers:

- Our method produces the output in the reflection angle at the reflector, and not in the offset ray-parameter. This makes the results more open to interpretation, and potentially allows for consistent quantitative AVA analysis.

- Our method generates angle gathers after and not during migration, thus enabling us to

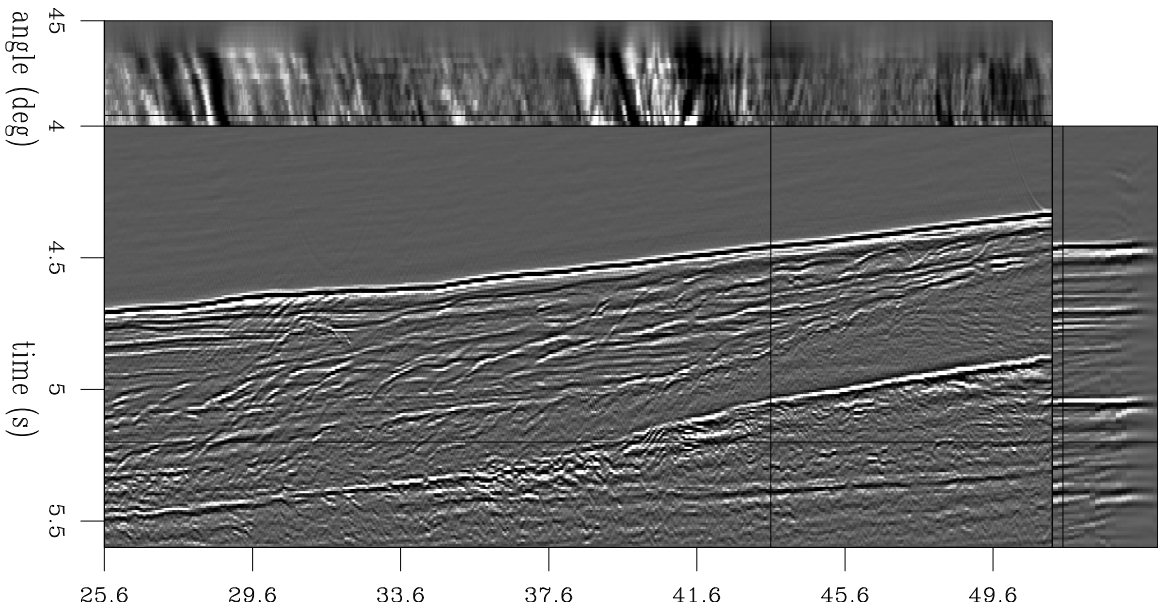

Figure 7: Migrated image for the gas-hydrates data presented as ADCIGs. agfft-hydrreal.cig [NR]

shuttle between the angle and offset domains without re-migrating the data. In addition, the method is much easier to code, and therefore potentially more robust.

- Our method enables inexpensive regularization of the angle-domain, leading to gathers with events that vary smoothly along the angle axis. The increased S/N ratio helps reveal weak events that would otherwise be impossible to find.

- If used in conjunction with prestack Stolt residual migration, the cost of our method becomes trivial, since the images are already transformed to the Fourier-domain. Also, returning to the space-domain after our transformation is less costly, since we reduce the need for a 3-D Fourier transform at every midpoint to that of a 1-D Fourier transform.

CONCLUSIONS

We have presented a method for computing angle-domain common-image gathers from wave-equation depth-migrated images. We have shown that the method is, in essence, a radial trace transform in the Fourier domain, and therefore equivalent to a slant stack in the space domain. We used a stretch technique that enabled us to include model regularization, which leads to smooth ADCIGs. We have also shown that the method is accurate, fast, robust, easy to implement and that it can be used for real 3-D prestack data in applications related to velocity and AVA analysis.

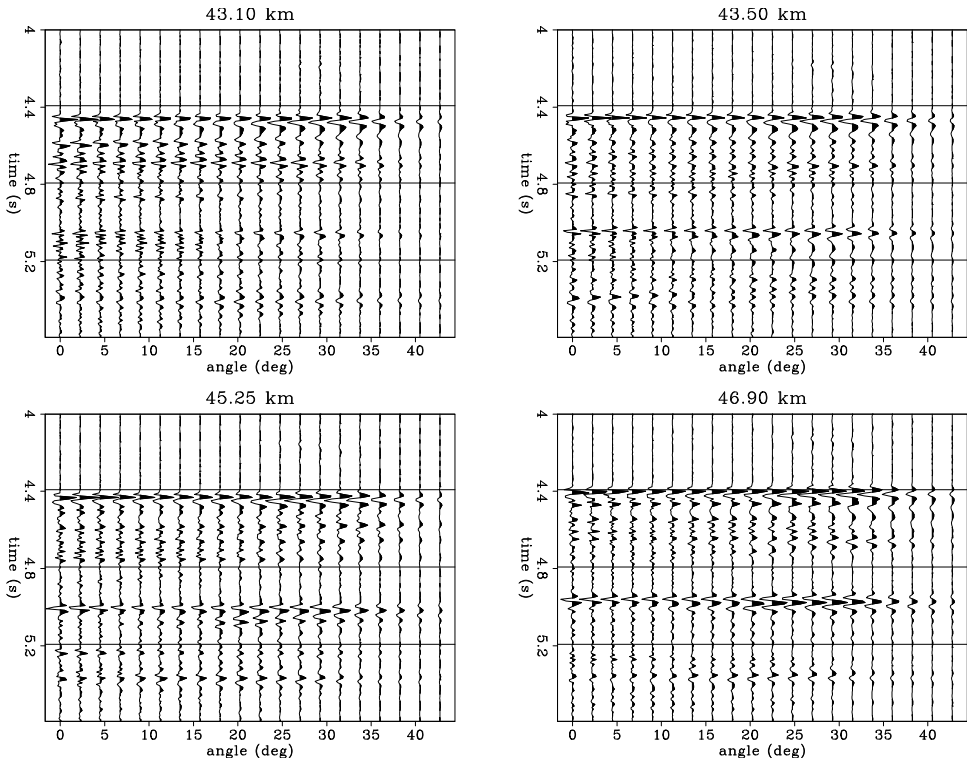

Figure 8: AVA analysis panels for the hydrates data. The BSR (located around 4.4 s) clearly shows consistent increase of the amplitude with angle and confirms previously reported results. Each panel is labeled with the horizontal coordinate of the image-gather. agfft-hydrreal.ava [NR]

ACKNOWLEDGMENT

Elf Aquitaine provided both the synthetic salt-dome model and the North Sea dataset.

REFERENCES

Biondi, B., and Sava, P., 1999, Wave-equation migration velocity analysis: 69th Ann. Internat. Meeting, Soc. Expl. Geophys., Expanded Abstracts, 1723–1726.

Biondi, B. L., 1999, 3-D Seismic Imaging: Stanford Exploration Project.

Brown, M., and Claerbout, J., 2000, Ground roll and the Radial Trace Transform - revisited: SEP–**103**, 219–237.

Ecker, C., 1998, Seismic characterization of methane hydrate structures: Ph.D. thesis, Stanford University.

Fomel, S., and Prucha, M., 1999, Angle-gather time migration: SEP–**100**, 141–150.

Fomel, S., 1998, Velocity continuation by spectral methods: SEP–**97**, 157–172.

Golub, G. H., and Van Loan, C. F., 1989, Matrix computations: The Johns Hopkins Press Ltd., London.

Ottolini, R., 1982, Migration of reflection seismic data in angle-midpoint coordinates: Ph.D. thesis, Stanford University.

Prucha, M. L., Clapp, R. G., and Biondi, B. L., 1998, Imaging under the edges of salt bodies: Analysis of an Elf North Sea dataset: SEP–**97**, 35–44.

Prucha, M., Biondi, B., and Symes, W., 1999a, Angle-domain common-image gathers by wave-equation migration: 69th Ann. Internat. Meeting, Soc. Expl. Geophys., Expanded Abstracts, 824–827.

Prucha, M. L., Biondi, B. L., and Symes, W. W., 1999b, Angle-domain common image gathers by wave-equation migration: SEP–**100**, 101–112.

Sava, P., and Biondi, B., 2000, Wave-equation migration velocity analysis: Episode II: SEP–**103**, 19–47.

Sava, P., 1999a, Short note–on Stolt common-azimuth residual migration: SEP–**102**, 61–66.

Sava, P., 1999b, Short note–on Stolt prestack residual migration: SEP–**100**, 151–158.

Vaillant, L., and Fomel, S., 1999, On stolt stretch time migration: SEP–**102**, 67–76.

Vaillant, L., and Sava, P., 1999, Common-azimuth migration of a North Sea dataset: SEP–**102**, 1–14.